

## Article

# A Study on the Weldment Hardening Discrimination Procedure and Improvement of Flux Cored Arc Welding Process of ASTM A553-1 (9% Nickel Steel) Material Using Bead Geometry Distribution

Minho Park <sup>1</sup>, Jisun Kim <sup>2</sup>, Changmin Pyo <sup>2</sup> , Jaewoong Kim <sup>2,\*</sup> and Kwangsan Chun <sup>3,\*</sup>

<sup>1</sup> Southwestern Branch Institute, Research Institute of Medium & Small Shipbuilding, Yeongam, Jeonnam 58457, Korea; mhpark@rims.re.kr

<sup>2</sup> Smart Manufacturing Process R&D Group, Korea Institute of Industrial Technology, Gwangju 61012, Korea; kimjisun@kitech.re.kr (J.K.); changmin@kitech.re.kr (C.P.)

<sup>3</sup> Industrial Application R&D Group, Welding Engineering R&D Department, Daewoo Shipbuilding & Marine Engineering Co., Ltd., Geoje-si 53302, Korea

\* Correspondence: kjw0607@kitech.re.kr (J.K.); kschun@dsme.co.kr (K.C.);  
Tel.: +82-62-600-6480 (J.K.); +82-62-600-6302 (K.C.)



**Citation:** Park, M.; Kim, J.; Pyo, C.; Kim, J.; Chun, K. A Study on the Weldment Hardening Discrimination Procedure and Improvement of Flux Cored Arc Welding Process of ASTM A553-1 (9% Nickel Steel) Material Using Bead Geometry Distribution. *Metals* **2021**, *11*, 1282. <https://doi.org/10.3390/met11081282>

Academic Editor: Pasquale Russo Spena

Received: 20 June 2021

Accepted: 10 August 2021

Published: 13 August 2021

**Publisher's Note:** MDPI stays neutral with regard to jurisdictional claims in published maps and institutional affiliations.



**Copyright:** © 2021 by the authors. Licensee MDPI, Basel, Switzerland. This article is an open access article distributed under the terms and conditions of the Creative Commons Attribution (CC BY) license (<https://creativecommons.org/licenses/by/4.0/>).

**Abstract:** As a result of strengthened sulfur content standards for ship fuel oil in IMO regulations, major domestic and foreign carriers have a high and growing demand for liquefied natural gas (LNG) powered ships and related equipment. For LNG operation in a cryogenic environment, a storage tank and fuel supply system that uses steel with excellent brittleness and fatigue strength is required. Ships that use LNG have a high vulnerability to explosion and fire. For this reason, 9% Ni is typically used, since a ship requires high quality products with special materials and structural technologies that guarantee operability at cryogenic temperatures. However, there is an urgent need for research to derive a uniform welding quality, since high process difficulty and differences in welding quality related to a welder's skills can cause a deterioration of the weld quality in the 9% Ni steel welding process. For 9% Ni steel, the higher the dilution ratio of the base metal, the lower the strength. In order to secure the required strength, excessive dilution of the base metal should be avoided, and the relationship between dilution ratio and strength should be investigated. According to previous research, if it exceeds 25% it may be lower than the API standard of 363 MPa for hardening welds. Therefore, in this study, the flux cored arc welding process is performed by establishing criteria that can be evaluated based on the SVM method in order to determine the structure of the weld to be cured according to the dilution rate of the base metal. We would like to propose a multipurpose optimization algorithm to ensure uniform quality of 9% Ni steel.

**Keywords:** flux cored arc welding; ASTM A553-1 (9% nickel steel); discriminant analysis; weldment hardening; optimization

## 1. Introduction

Since January 2020, the International Maritime Organization (IMO) has been applying a stricter standard for the sulfur content of ship fuel oil, finally announcing a plan to restrict the sulfur content of ship fuel oil from the current level of 3.5% to 0.5% in 2020. Around the world, each country has legislated the IMO 2020 standards, and is applying more stringent regulations to voluntarily designated emission control areas rather than other sea areas. Major domestic and international carriers are complying with IMO's strict environmental regulations by considering the pros and cons of various alternatives such as installing a scrubber, using low-sulfur oil, or using LNG.

As eco-friendliness has become an international trend, a dramatic energy transition is taking place around the world and the demand for liquefied natural gas (LNG) is also

increasing in the shipping sector. The bunkering industry (i.e., refueling LNG to LNG-powered ships), is also emerging around the world. The equipment applied to an LNG propulsion ship can be broadly divided into engines, fuel tanks, fuel supply systems, and fuel supply control systems. A shipbuilder or shipowner makes an order in a packaged type, in which a tank or supply system can be directly installed onto a ship. However, high-quality products with special materials and structural technologies for cryogenic operability are needed, since operational disruption or anchoring due to equipment failure can cause significant economic losses [1–4].

The LNG storage tank has a cryogenic structure, and 9% Ni steel (which has excellent mechanical properties and fatigue strength at room temperature as well as in low temperature environments) is most often used as the material for the inner tank. The 9% Ni steel has excellent impact toughness and fatigue strength in a cryogenic environment, and is widely used in the production of LNG storage tanks due to its low material price compared to steel density. When using 9% Ni steel, it is recommended the absorption energy specified in domestic and international regulations should be 34 J or more at  $-196\text{ }^{\circ}\text{C}$ . However, there are slight differences depending on the standard actually applied. INCO (International Nickel Co., Ltd., New York, NY, USA) in the United States first developed 9% Ni steel in 1944, and more recently Japan has been at the forefront of improvements in steel quality, developing welding technology, and continuing research on safety considering the trend of larger tank sizes [5,6].

The welding process of 9% Ni steel is very difficult for field engineers due to the difference between the melting point of the base metal and the welding wire. This represents the hurdle for using 9% Ni steel in its many applications. Thus, this research focuses on the determination of welding performance and suggests the optimal welding condition.

Since the welding material has a lower melting point than a base material and the welding quality is different depending on the welder's skills, A553-1 steel welding is not easy. Therefore, it is necessary to review the issues that might occur during the welding of A553-1 steel and to prevent welding defects by evaluating the characteristics of the weldment.

This study focused the specific welding method and a material, FCAW and 9% nickel steel. For analyzing the welding quality, the hardness of the upper welding part after welding (which is known to be vulnerable to cracks due to 'weldment hardening') was defined. Furthermore, that concept was used as an output variable for determination formula in order to evaluate the welding quality. Many parameters related to the welding process were used as input variables. By optimizing those input variables based on that determination formula and multi objective optimization algorithm, improved welding qualities were obtained.

This study was related the previous research which evaluated the weldability with solidification crack susceptibility [7], and used similar evaluating methods such as welding test and optimization. However, it focused on weldment hardening as an evaluating method differently.

Naturally, the previous studies are similar to past research [7]. Yun [8] performed the optimization of fillet laser welding for 9% Ni steel, and Na [9] compared GTAW and FCAW for 9% Ni steel. Kim [10] designed the LNG fueled ship with 9% Ni steel and evaluated the welding performance. Watanabe [11] performed a double tension test for a surface notch of A553-1 steel. X Liu et al. [12] performed a study to measure and analyze the fracture toughness of metals by using machine learning models such as regression trees and neural networks. Oliveira [13,14] evaluated the mechanical properties that changed according to the micro-evolution occurring in the gas tungsten arc welding process, analyzed the process of material ductility by the refined grain structure in the fusion zone, and studied how low hardness can cause breakage. Kim evaluated the GMA welding performance with deep learning methods [15], and Zhu used deep learning-based classification for checking the defects of weld surface [16].

In previous studies, the correlation between diverse variables and mechanical characteristics applied to the welding process of cryogenic steels such as STS series or Ni alloy series has been reviewed and the process problems and quality deterioration that occurred when those were used in the LNG-related equipment were also reviewed. However, the previous research on weldment quality in cryogenic steel has not reflected the complex alternating effects, and most studies concern the application of automation, high melting, or high speeds to compensate for the disadvantages of manual welding [17,18]. In addition, research on the correlation between bead geometry and weldability has been performed in previous studies to improve welding quality by establishing the key factors affecting bead formation. However, similar size areas and heat-affected zones are derived intermittently even for different welding process variables, so the applicability of analysis and consideration limited to bead geometry in the actual field has been reduced.

In this way, an analysis based on various perspectives is needed to clearly identify the specific conditions that can have a similar bead geometry compared to the intermittent variables, and it is necessary to identify the phenomenon in which the structure of a weldment is hardened by matching the characteristics generated from the correlation between the partially divided bead geometry within a weldment to the dilution ratio of a weldment.

In 9% Ni steel, a higher dilution ratio of the base material leads to lower strength. For this reason, to guarantee the required strength, excessive dilution of the base material should be avoided. Although prior studies on the correlation between dilution ratio and strength have found that tensile strength does not change dramatically even when there is 10–20% change in the dilution ratio, it has been reported that strength may drop below the API standard of 363 MPa due to the hardening of the weldment if the dilution ratio is 25% or more [19,20].

Therefore, in this study, the dilution ratio formed in the weldment was calculated for the flux cored arc welding process applied to 9% Ni, a cryogenic steel, and the phenomenon in which a hardened weldment is created compared to the heat-affected zone was identified in a procedure based on the calculated dilution ratio. This study tried with purpose a method for quantitatively evaluating the quality of weldments. Therefore, the bead geometry, hardness, and dilution rate were analyzed for the welded part (which was tested by applying various process variables), and the correlation of the tendency of the quality of the welded part to deteriorate was derived. In addition, the raw data collected to quantify the quality deterioration characteristics of the collected welds was trained by the discriminant function. The effects contained in the process variables were predicted, and the quality deterioration characteristics were based on the process variables [21–23]. If this as expected, we have also proposed a multipurpose algorithm that can be systematically avoided.

## 2. Experimental Works

A flux cored arc welding experiment was carried out to determine the quality of flux cored arc weld of 9% Ni steel and to develop the optimal process parameters. For the experiment, a 600A class FCAW welding machine (ProPAC, HYOSUNG, Mapo-gu, Seoul, Korea) and torch, a welding feeder, a straight welding carriage, and a guide rail were configured, and the overall system was arranged as shown in Figure 1.

The specimen was cleaned with ethyl alcohol (DUKSAN, Ansan-si, Gyeonggi-do, Korea) and sandpaper to prevent foreign substances such as rust, scale, and oxide from causing welding defects on the surface of a specimen to be welded. Figure 2 shows the schematic diagram of a flux cored arc welding process. The test piece used in the welding test was used in a size of 150 mm (W) × 200 mm (H) × 15 mm (H) of 9% Ni steel (NIPPON STEEL, Chiyoda City, Tokyo, Japan). The mechanical properties and chemical composition of the 9% Ni steel and wire used in the flux cored arc welding test are shown in Tables 1 and 2, respectively.



Figure 1. Experimental setup for flux cored arc welding [7].

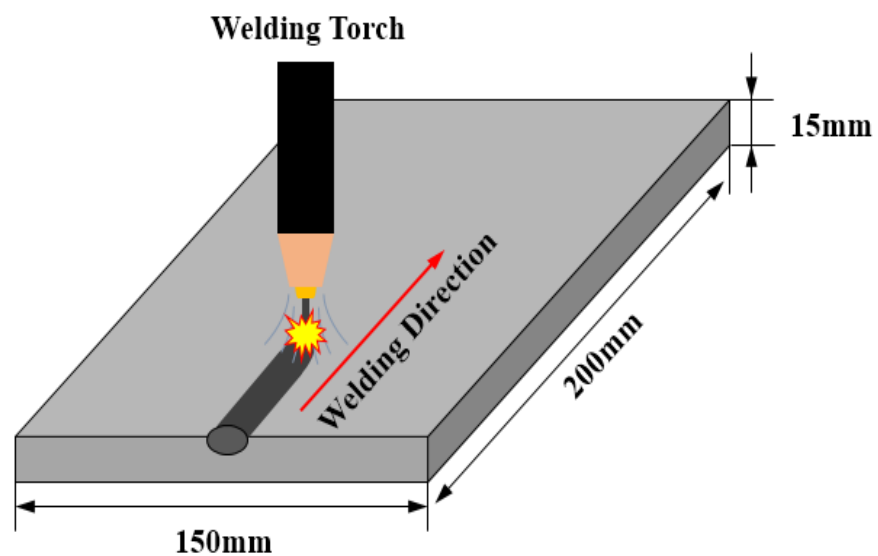


Figure 2. Schematic diagram for the flux cored arc welding process [7].

Table 1. Mechanical properties of base metal [7].

Material	Yield Strength (MPa)	Tensile Strength (MPa)	Elongation (%)	Hardness (HV)
A553-1	651.6	701.1	26.6	243.0
Welding Wire	460.0	730.0	47.0	230.0

Table 2. Chemical composition of base metal [7].

Material	C	Si	Mn	S	P	Ni	Fe
A553-1	0.05	0.67	0.004	0.003	0.25	9.02	Bal.
Welding Wire	0.02	0.02	0.1	0.001	0.001	69.8	5.6

The selected input variables of flux cored arc welding applied in this experiment were welding current, arc voltage, and welding speed, which have a clear influence on the bead geometry and weldability of GMA weldment. To analyze the weldability, bead geometry and mechanical properties such as heat-affected zone and weldment hardness were collected [11]. Figure 3 shows the schematic diagram for the measurement of a penetration bead of the weldment.

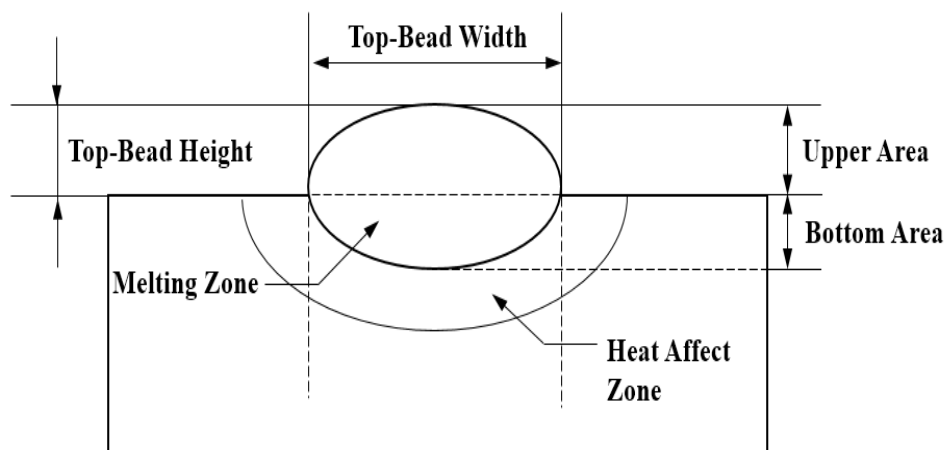


Figure 3. Schematic diagram of bead geometry [7].

In this experiment, it is possible to estimate all factor effects for the response of an output variable according to the change of an input variable, and the full factorial placement method (FFD) was applied to detect the correlation effect of higher orders. The appropriate level and range of input variables (welding current, arc voltage, welding speed) were selected from preliminary experiments. A total of 18 experimental conditions were created from  $3^2 \times 2$  (three welding current, three arc voltage, and two welding speed). Tables 3 and 4 show the experimental variables and levels of the input variables and the experimental conditions for a total of 18 trials.

Table 3. Flux cored arc welding parameters and their levels [7].

Parameter	Symbol	−1	0	1
Welding Current (A)	C	150	160	170
Arc Voltage (V)	V	21	23	25
Welding Speed (meter/minute, m/min)	S	0.3	—	0.4
Fixed Parameter		Welding Wire: $\varnothing$ 1.2 Flux Wire Contact Tip Work Distance: 15 mm Shielding Gas Flow Rate: CO <sub>2</sub> 18 L/min		

Table 4. Experimental plan of flux cored arc welding process [7].

Test No.	C	V	S	Test No.	C	V	S
1	150	21	0.3	10	150	21	0.4
2	150	23	0.3	11	150	23	0.4
3	150	25	0.3	12	150	25	0.4
4	160	21	0.3	13	160	21	0.4
5	160	23	0.3	14	160	23	0.4
6	160	25	0.3	15	160	25	0.4
7	170	21	0.3	16	170	21	0.4
8	170	23	0.3	17	170	23	0.4
9	170	25	0.3	18	170	25	0.4

### 3. Results

#### 3.1. Measurement of Bead Geometry

BOP flux cored arc welding of 9% Ni steel, which is a cryogenic steel, was performed properly according to the process parameters. In the result of the experiment, it was confirmed that a good weldment was formed in general and there were no pores or defects in appearance. To properly represent the cross-sectional appearance of a specimen, 90% Ethanol + 10% Nitric solution was mixed and used to etch the cross-section. An optical microscope system was used to measure the bead geometry accurately. Table 5 shows the welding cross-section and bead measurement results taken with a 10X optical microscope (Sometch, Seoul, Korea).

**Table 5.** Results of flux cored arc welding experiment [7].

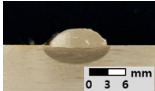
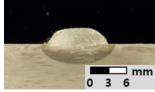
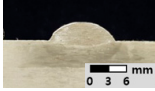
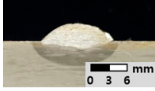
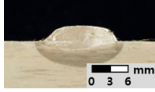

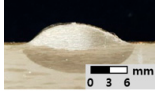
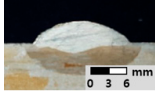
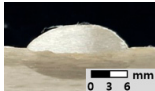
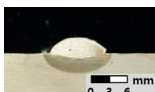
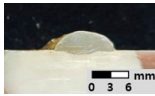
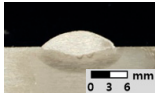
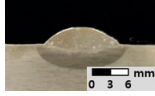





Test No.	Top-Bead Width (mm)				Top-Bead Height (mm)				Bead Geometry
	1st	2nd	3rd	Average	1st	2nd	3rd	Average	
1	8.46	8.47	8.46	8.46	2.58	2.61	2.59	2.59	
2	8.91	8.85	8.88	8.88	2.83	2.82	2.84	2.83	
3	9.64	9.63	9.63	9.63	2.85	2.83	2.88	2.86	
4	10.25	10.25	10.28	10.26	2.82	2.80	2.77	2.80	
5	10.82	10.81	10.81	10.81	2.94	2.96	2.92	2.94	
6	11.19	11.18	11.18	11.18	3.09	3.10	3.10	3.10	
7	11.43	11.44	11.43	11.43	3.12	3.11	3.09	3.11	
8	12.09	12.13	12.14	12.12	3.17	3.14	3.19	3.17	
9	13.28	13.31	13.30	13.30	3.26	3.26	3.24	3.25	
10	8.57	8.58	8.56	8.57	2.75	2.76	2.74	2.75	



Table 5. Cont.

Test No.	Top-Bead Width (mm)				Top-Bead Height (mm)				Bead Geometry
	1st	2nd	3rd	Average	1st	2nd	3rd	Average	
11	9.56	9.53	9.45	9.51	2.85	2.86	2.90	2.87	
12	9.70	9.71	9.64	9.68	2.89	2.91	2.91	2.90	
13	10.32	10.35	10.38	10.35	2.88	2.89	2.87	2.88	
14	10.88	10.84	10.81	10.84	2.89	2.92	2.94	2.92	
15	11.38	11.35	11.32	11.35	3.09	3.09	3.08	3.09	
16	12.06	12.05	12.09	12.07	3.13	3.12	3.11	3.12	
17	12.97	12.96	12.94	12.96	3.21	3.19	3.17	3.19	
18	13.42	13.40	13.41	13.41	3.27	3.28	3.31	3.29	

### 3.2. Measurement of Weldment Hardness

A hardness test was performed on each specimen to confirm the hardening phenomenon of a weldment where there is a change of internal strength and structure due to the difference in the concentration of the arc force and the electromagnetic force when the flux cored arc weldment was solidified. To determine the hardness of a weldment, the Vickers hardness test was performed on the upper and lower parts and the heat-affected zone where the change in internal strength occurs. The load used in the hardness test was selected as 0.5 N and analysis was performed at 0.83 mm intervals so as not to affect the nearby hardness. Figure 4 shows the schematic diagram of the hardness test for the weldment of 9% Ni steel. Table 6 shows the test results for the hardness of upper and lower parts of a weldment and the heat-affected zone. The hardness test result means the average value measured at 5 points. The hardness (lower part) of a flux cored arc weldment shows a value between 286.1 HV0.05 and 291.9 HV0.05, which is higher than the 243 HV0.05 hardness which is a 9% Ni steel standard. Therefore, it is judged that sufficient weldability is achieved.

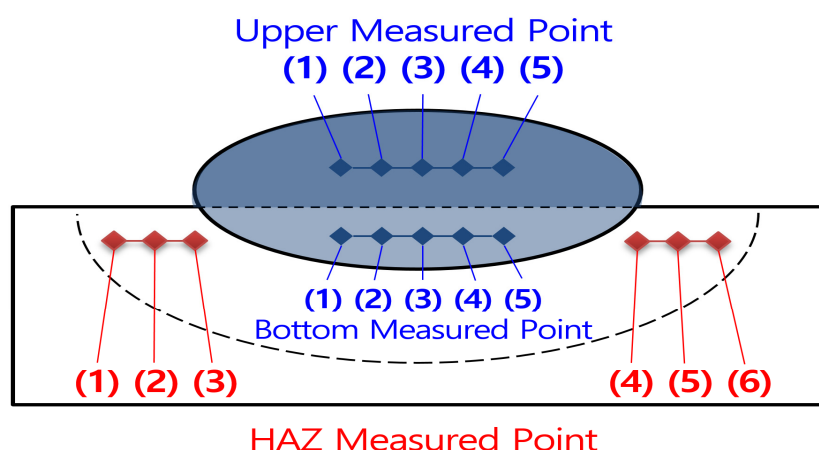


Figure 4. Schematic diagram of the hardness test.

Table 6. Results of hardness according to welding process and parameters.

Test No.	Upper by Point (HV0.05)		Bottom by Point (HV0.05)		HAZ by Point (HV0.05)	
	Average	Standard Deviation	Average	Standard Deviation	Average	Standard Deviation
1	253.3	2.2	286.1	2.3	328.9	0.5
2	250.1	2.3	287.0	3.6	333.7	0.7
3	251.9	1.0	288.3	2.9	336.9	0.3
4	255.1	1.8	287.5	0.1	341.2	0.1
5	259.6	2.2	289.7	0.3	340.5	0.3
6	254.7	1.7	290.7	0.5	340.7	0.5
7	261.7	3.7	290.9	0.4	343.8	0.4
8	262.6	2.3	291.2	0.4	349.9	0.6
9	261.5	1.6	291.9	4.9	346.6	0.4
10	259.1	2.7	286.7	0.4	337.1	0.6
11	260.2	2.9	287.6	1.8	336.3	0.3
12	254.6	1.0	287.5	1.7	334.9	0.5
13	255.8	1.7	288.4	2.4	338.8	0.2
14	258.6	1.5	289.1	3.8	342.9	0.4
15	259.1	1.6	289.2	1.7	342.6	0.4
16	261.3	3.8	291.5	0.3	346.2	0.6
17	251.9	2.6	287.7	2.1	336.6	0.7
18	256.3	2.2	287.2	2.5	342.8	0.7

### 3.3. Measurement of Weldment Dilution Ratio

The bead geometry of a flux cored arc welding process varies depending on the changes in arc force and heat input caused by differences in welding current, arc voltage, and wire supply speed. There is a very high possibility that hardening will occur due to a change in the chemical composition and internal strength of the weldment. In this way, the characteristics from the correlation between the bead geometry and the quality characteristics of a weldment were matched to the dilution ratio of a weldment in order to analyze the phenomenon of hardening of a weldment structure.

Figure 5 shows the schematic diagram to calculate the weldment dilution ratio of a flux cored arc welding process and Figure 6 shows the picture of calculating a weldment dilution ratio using the area analysis tool in the system via an optical microscope. Table 7 shows the dilution ratio of the weldment area according to the flux cored arc welding process parameters.



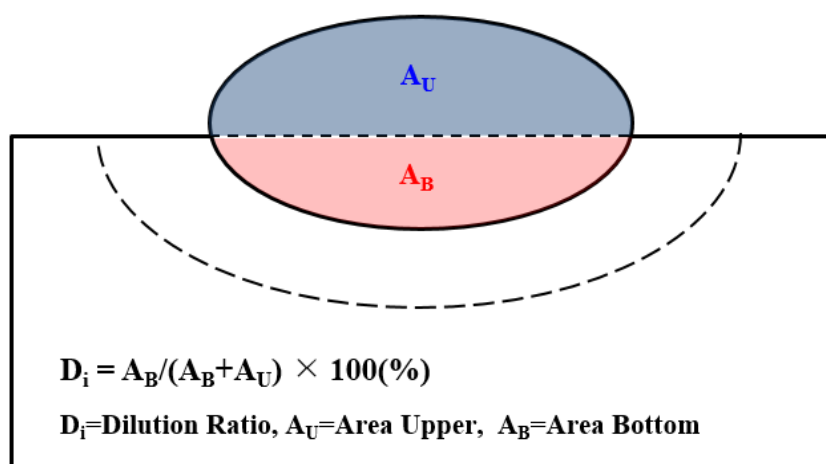


Figure 5. Schematic diagram of dilution ratio.

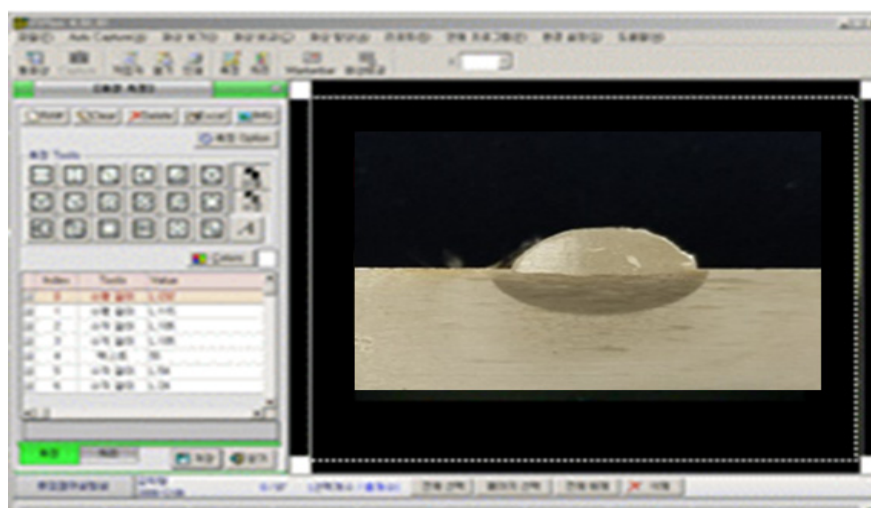


Figure 6. Optical microscope for dilution ratio measurement.

Table 7. Results of dilution ratio for flux cored arc welding.

Test No.	Avg. Area Upper (mm <sup>2</sup> )	Avg. Area Bottom (mm <sup>2</sup> )	Dilution Ratio (%)	Test No.	Avg. Area Upper (mm <sup>2</sup> )	Avg. Area Bottom (mm <sup>2</sup> )	Dilution Ratio (%)
1	16.9	3.17	15.81	10	18.63	3.06	14.11
2	19.19	3.75	16.34	11	21.6	3.38	13.53
3	21.35	3.97	15.69	12	21.97	4.1	15.74
4	22.65	3.63	13.81	13	23.06	4.08	15.04
5	25.48	4.08	13.82	14	25.17	4.05	13.87
6	26.92	5.3	16.46	15	27.52	4.57	14.24
7	28.09	4.88	14.8	16	29.55	4.75	13.85
8	30.32	4.7	13.43	17	32.32	6.25	16.19
9	34.65	5.81	14.36	18	34.13	5.99	14.92

#### 4. Discriminant of Quality Characteristics of 9% Ni Steel

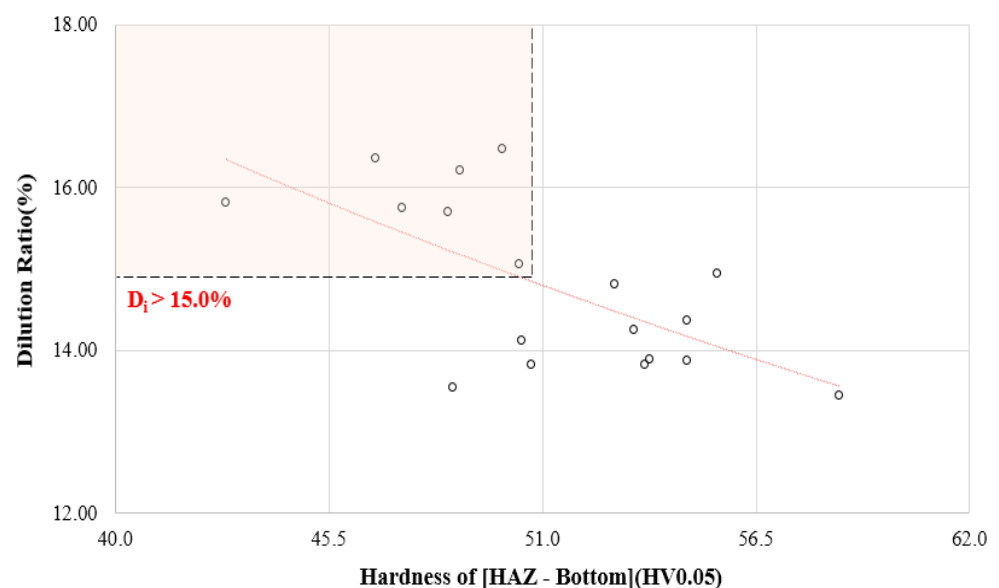
##### 4.1. Weldment Hardening According to Dilution Ratio

In 9% Ni steel, a higher dilution ratio of the base material results in lower strength. To secure the required strength, excessive dilution of the base material should thus be avoided. Although prior studies on the relationship between dilution ratio and strength have found that the tensile strength does not change significantly even when there is 10–20% change in dilution, it has been reported that it may be lower than the API standard of 363 MPa due to hardening of a weldment if dilution is 25% or more [19,20]. In addition, even under different welding conditions, the level of hardening of heat-affected zones is similar when

the amount of heat input is the same. However, the electromagnetic force and the energy density of the beam are different, so the effect on bead formation is also different. This leads to a disadvantage of increased hardness of a weldment compared to the heat-affected zone. To address the shortcomings of prior studies that established the characteristics of a welding process limited to bead geometry as described above, the correlation between dilution concept and strength of a weldment was established.

Therefore, in this section, the dilution ratio formed in a weldment is calculated for each welding process and process variable and a standard for the generation of a weldment hardened compared to the heat-affected zone is established according to the calculated dilution ratio in order to set up a stable weldment dilution ratio standard.

To analyze the correlation of hardness based on the dilution ratio that changes according to the bead geometry, we attempted to establish a standard for hardening or scattering of the lower weldment compared to the heat-affected zone. The difference and trend between the measured hardness of the heat-affected zone and the hardness of the lower weldment were used to set up a dilution ratio standard that can avoid hardening of a weldment, as shown in Figure 7. As a result, the degree of hardness (i.e., the difference between the hardness of heat-affected zone and the hardness of lower weldment) of a flux cored arc weldment was between 42.8 HV0.05 and 58.7 HV0.05 and the difference in hardness of a weldment was confirmed to be 42.8 HV0.05 or lower compared to the heat-affected zone (when the dilution ratio of weldment was calculated to be 15.0% or more). It was thus confirmed that the difference in hardness compared to the heat affected zone was not high as the dilution ratio was increased. It was judged that if there is this kind of hardening of a weldment, it is difficult to secure the quality against the brittle effect and durability.



**Figure 7.** Weldment hardening according to dilution ratio in flux cored arc welding.

The standard of a 15.0% dilution ratio confirmed above is a standardized score, and can be used as an evaluation index for the process. When a high score is calculated, it means that a hardened structure of a weldment is created. Therefore, the criteria for determining the hardening of a weldment can be defined as shown in Table 8. These standardized scores can be later applied as learning data to determine the increase in weldment hardness and brittleness according to the bead geometry and dilution ratio. We attempted to prevent the generation of hardened structure and deterioration of weldment strength due to arc electromagnetic force at 9% Ni steel weldment where the welding process was applied.

**Table 8.** Weldment hardening data for discriminant analysis in flux cored arc welding.

Test No.	Hardness Difference (HV0.05)	Dilution Ratio (%)	Weldment Hardening	Test No.	Hardness Difference (HV0.05)	Dilution Ratio (%)	Weldment Hardening
1	42.9	15.81	Regard	10	50.5	14.11	Regardless
2	46.7	16.34	Regard	11	48.7	13.53	Regardless
3	48.6	15.69	Regard	12	47.4	15.74	Regard
4	53.7	13.81	Regardless	13	50.4	15.04	Regard
5	50.7	13.82	Regardless	14	53.8	13.87	Regardless
6	50.0	16.46	Regard	15	53.4	14.24	Regardless
7	52.9	14.80	Regardless	16	54.7	13.85	Regardless
8	58.7	13.43	Regardless	17	48.9	16.19	Regard
9	54.7	14.36	Regardless	18	55.5	14.92	Regardless

#### 4.2. Discriminant Analysis

The system to determine weldment hardening in the flux cored arc welding process of 9% Ni steel is a technique used to determine the affiliation of the input data by making a model using the collected data and entering it into the developed group learning data [24–26].

For the weldment hardening system to be developed in this study, a discriminant model was developed using the SVM (Support Vector Machine) technique. In the problem of finding the hyperplane that maximizes a margin in the two classes where linear discrimination is possible based on the VC (Vapnik–Chervonenkis) theory and Equation (1), this study tried to determine the possibility of hardening of a weldment in the process [27].

$$w \cdot x + b = 0 \quad (1)$$

The variables for learning in the weldment hardening discrimination model are welding process variables (welding current, arc voltage, welding speed), bead geometry (top-bead width, top-bead height), upper and bottom hardness, heat affected zone hardness (HAZ hardness), and dilution ratio. One hundred and eighty data points were entered with a total of 10 multiple variables. For the groups used to determine the hardening of a weldment, the Regard Group was defined as 1 and the Regardless Group was defined as 0, to confirm the discrimination performance predicted based on the SVM technique.

Table 9 shows the learning data to discriminate the hardening of a weldment and Table 10 and Figure 8 quantitatively show the group discrimination performance which was predicted by the data learned in the SVM technique.

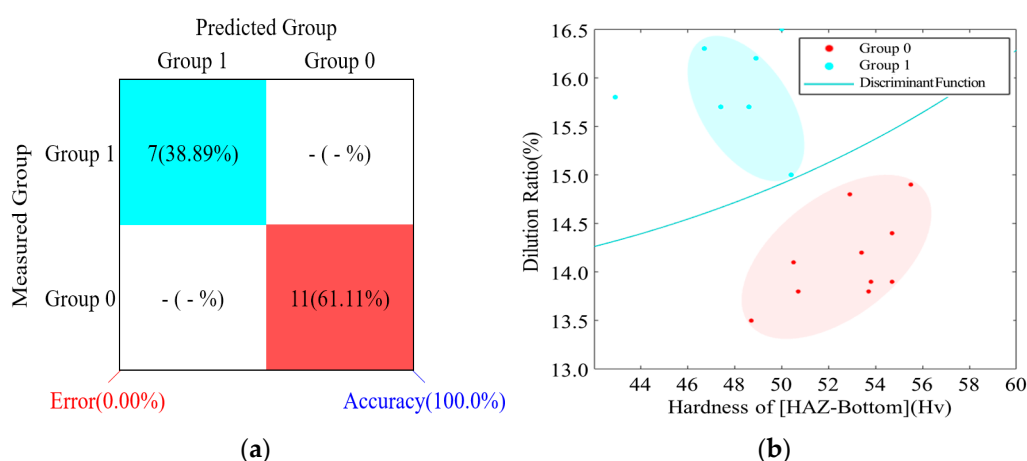
**Table 9.** Learning data for discriminant of flux cored arc welding quality.

Test No.	C	V	S	W	H	H <sub>U</sub>	H <sub>B</sub>	H <sub>H</sub>	D <sub>i</sub>	Group
1	150.0	21.0	0.3	8.46	2.59	253.3	286.1	328.9	15.8	Regard
2	150.0	23.0	0.3	8.88	2.83	250.1	287.0	333.7	16.3	Regard
3	150.0	25.0	0.3	9.63	2.86	251.9	288.3	336.9	15.7	Regard
4	160.0	21.0	0.3	10.26	2.80	255.1	287.5	341.2	13.8	Regardless
5	160.0	23.0	0.3	10.81	2.94	259.6	289.7	340.5	13.8	Regardless
6	160.0	25.0	0.3	11.18	3.10	254.7	290.7	340.7	16.5	Regard
7	170.0	21.0	0.3	11.43	3.11	261.7	290.9	343.8	14.8	Regardless
8	170.0	23.0	0.3	12.12	3.17	262.6	291.2	349.9	13.4	Regardless
9	170.0	25.0	0.3	13.30	3.25	261.5	291.9	346.6	14.4	Regardless
10	150.0	21.0	0.4	8.57	2.75	259.1	286.7	337.1	14.1	Regardless
11	150.0	23.0	0.4	9.51	2.87	260.2	287.6	336.3	13.5	Regardless
12	150.0	25.0	0.4	9.68	2.90	254.6	287.5	334.9	15.7	Regard
13	160.0	21.0	0.4	10.35	2.88	255.8	288.4	338.8	15.0	Regard
14	160.0	23.0	0.4	10.84	2.92	258.6	289.1	342.9	13.9	Regardless
15	160.0	25.0	0.4	11.35	3.09	259.1	289.2	342.6	14.2	Regardless
16	170.0	21.0	0.4	12.07	3.12	261.3	291.5	346.2	13.9	Regardless
17	170.0	23.0	0.4	12.96	3.19	251.9	287.7	336.6	16.2	Regard
18	170.0	25.0	0.4	13.41	3.29	256.3	287.2	342.8	14.9	Regardless

C, Welding Current (A); V, Arc Voltage (V); S, Welding Speed (m/min); W, Top-Bead Width (mm); H, Top-Bead Height (mm); H<sub>U</sub>, Upper Hardness (HV0.05); H<sub>B</sub>, Bottom Hardness (HV0.05); H<sub>H</sub>, HAZ Hardness (HV0.05); D<sub>i</sub>, Dilution Ratio (%).

**Table 10.** Results of group discriminant for weldment hardening according to SVM.

Test No.	Measured Group	Predicted Group	Test No.	Measured Group	Predicted Group
1	1	1(1.00)	10	0	0(0.00)
2	1	1(1.00)	11	0	0(0.00)
3	1	1(1.00)	12	1	1(1.00)
4	0	1(0.00)	13	1	1(0.69)
5	0	0(0.00)	14	0	0(0.00)
6	1	1(1.00)	15	0	0(0.00)
7	0	0(0.00)	16	0	0(0.00)
8	0	0(0.00)	17	1	1(1.00)
9	0	0(0.00)	18	0	0(0.03)

**Figure 8.** Weldment hardening discriminant in flux cored arc welding: (a) Performance evaluation for SVM and (b) Discriminant graph for SVM.

## 5. Optimization of Flux Cored Arc Welding of 9% Ni Steel

### 5.1. Development of Mathematical Model Welding Factors

The response surface analysis method is a statistical analysis method for the response surface formed by the change of response when several input variables  $x_1, x_2, x_3, \dots, x_k$  have an effect on the output variable  $y$  through complex actions. This procedure was carried out in the previous research [7].

The functional relationship between the input variables  $x_1, x_2, x_3, \dots, x_k$  and the output variable  $y$  is expressed by Equation (2). Considering the predictive ability of linear and nonlinear models, Equation (3) is expressed as a second order regression model if it is assumed the predicted value of the output variable (i.e., the welding factor) has a linear relationship with an input variable.

$$Y_i = f(x_1, x_2, x_3) \quad (2)$$

$$Y_i = \beta_0 + \sum_{i=1}^k \beta_i x_i + \sum_{i \leq j}^k \beta_{ij} x_i x_j + \epsilon \quad (3)$$

Equation (3) can be arranged as Equation (4) by the least squares method.

$$\hat{Y}_i = \hat{\beta}_0 + \sum_{i=1}^k \hat{\beta}_i x_i + \sum_{i \leq j}^k \hat{\beta}_{ij} x_i x_j + c \quad (4)$$

In this study, Equation (4) can be expanded as Equation (5) since the number of input variables is 3, that is,  $k = 3$ .

$$\hat{Y}_i = \hat{\beta}_0 + \hat{\beta}_1 x_1 + \hat{\beta}_2 x_2 + \hat{\beta}_3 x_3 + \hat{\beta}_{11} x_1^2 + \hat{\beta}_{22} x_2^2 + \hat{\beta}_{33} x_3^2 + \hat{\beta}_{12} x_1 x_2 + \hat{\beta}_{13} x_1 x_3 + \hat{\beta}_{23} x_2 x_3 \quad (5)$$

where,  $\hat{Y}_i$  is the estimator of welding characteristics,  $x_i$  is the code unit of input variables (welding process variables and mechanical properties),  $\hat{\beta}_0$ ,  $\hat{\beta}_i$ ,  $\hat{\beta}_{ij}$  are the min. square estimators of  $\beta_0$ ,  $\beta_i$ ,  $\beta_{ij}$ , respectively, and  $\epsilon$  represents an error. To develop Equation (5) of the above regression model, it is necessary to obtain relevant data through multiple experiments.

To obtain relevant data through experiments in this way, numerous trials and errors may occur, resulting in economic losses. To reduce these losses, a full factorial design was applied among the response surface analysis methods of the DOE method that well reflects the second order regression model, and the coefficients of each term were calculated using MINITAB.

The mathematical prediction models of bead geometry (top-bead width, top-bead height), upper and bottom hardness, HAZ hardness, and dilution ratio developed using regression coefficients and Equation (5) can be expressed using Equations (6)–(11).

$$W = 4.0366 - 0.1264C + 0.0546V - 8.5917S + 0.0004C^2 - 0.0115V^2 + 0.0058CV + 0.1333CS - 0.4250VS \quad (6)$$

$$H = 2.1259 - 0.0802C + 0.3100V + 8.3833S + 0.0004C^2 - 0.0021V^2 - 0.0007CV - 0.0283CS - 0.1500VS \quad (7)$$

$$H_U = 1386.8 - 1.6263C - 232.99W + 2017.2H + 0.0186C^2 - 9.6578W^2 - 621.11H^2 - 0.2596CW - 0.3473CH + 161.33WH \quad (8)$$

$$H_B = 474.98 + 1.5594C + 8.0201W - 246.75H - 0.0325C^2 - 0.9159W^2 - 18.652H^2 + 0.1329CW + 2.5075CH - 3.3364WH \quad (9)$$

$$H_H = -1727.9 + 13.931C - 215.88W + 1385.1H - 0.0369C^2 - 7.8645W^2 - 328.98H^2 + 0.6200CW - 2.7470CH + 95.326WH \quad (10)$$

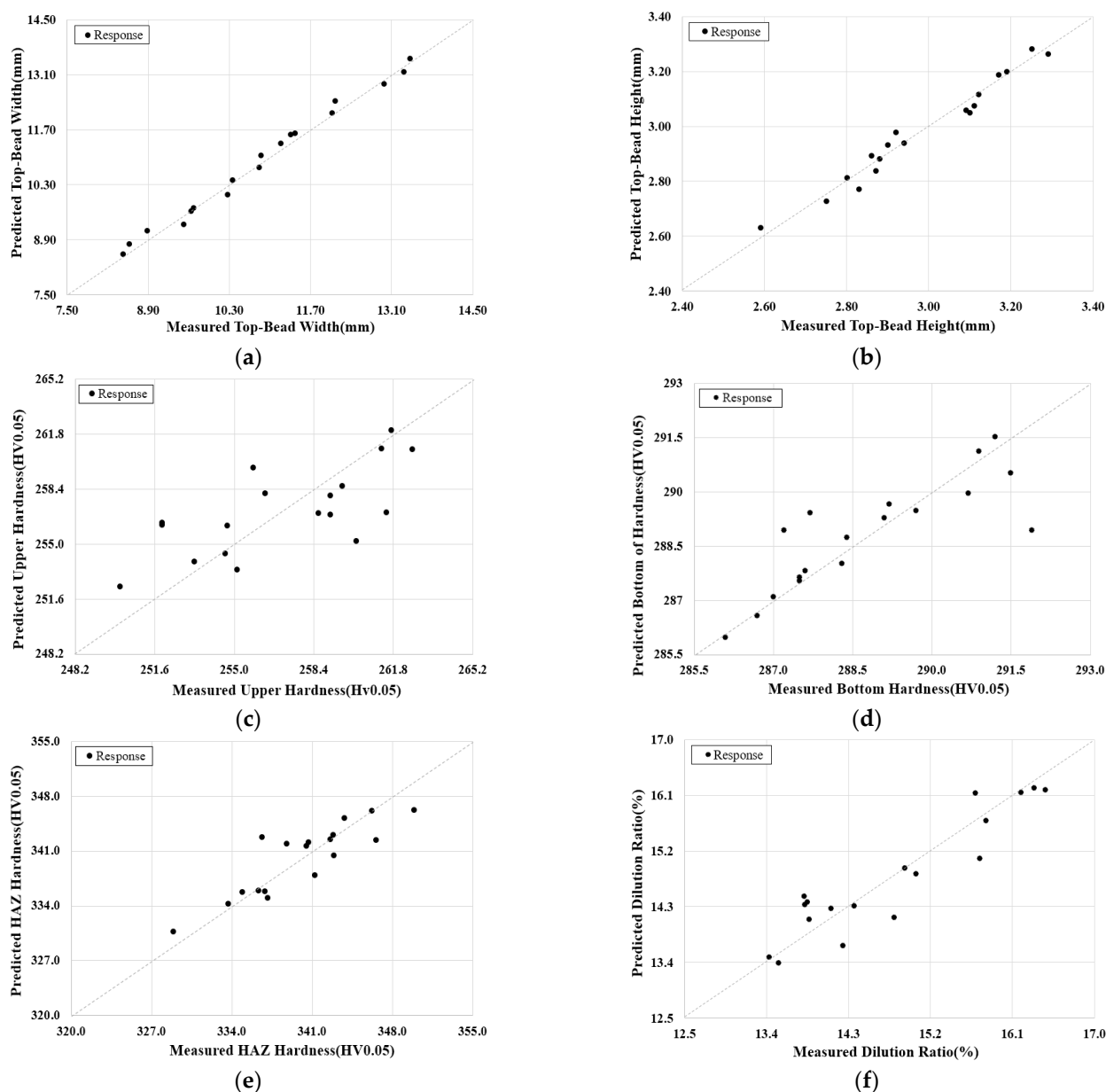
$$D_i = 4340.9 + 59.99W - 28.32H_B - 4.8825H_U + 0.3180W^2 + 0.0298H_B^2 - 0.0206H_U^2 - 0.1902WH_B - 0.0489WH_U + 0.0542H_BH_U \quad (11)$$

To check the predictive ability of the developed mathematical prediction model, the graph showing the error range by comparing the average value of measured welding factors for each experimental condition with the predicted welding factors is shown in Figure 9. As shown in Table 11, the prediction model error range showed reliable results in general.

In addition, the ANOVA (analysis of variance) results of the predictive model confirmed a high coefficient of determination of 98.9% at the maximum bead width and a minimum coefficient of determination of 72.4% at the bottom hardness of a weldment. This means that it is possible to predict by using the coefficient of determination for the entire variation of welding factors, and the interaction as well as the independent influence of input variables affecting the regression model are considered simultaneously.

**Table 11.** Analysis variance tests for predicted model for welding factors.

Design Parameter	SE (Standard Error)	R <sup>2</sup> (Coefficient of Determination, %)
$W$	0.221	98.9
$H$	0.046	96.9
$H_U$	0.098	73.0
$H_B$	1.436	72.4
$H_H$	3.697	76.2
$D_i$	0.572	85.4

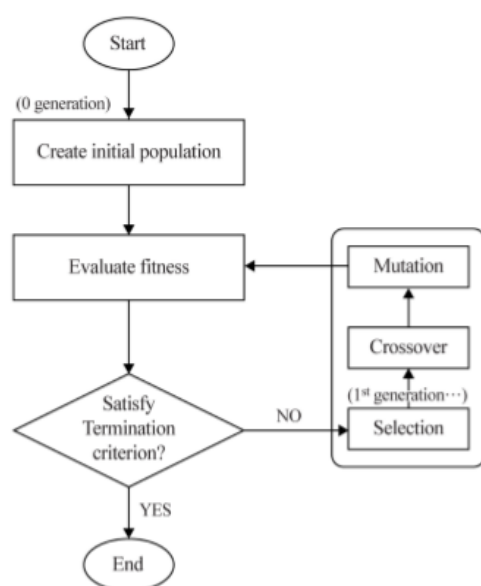


**Figure 9.** Comparison between measured and predicted welding factors according to mathematical model: (a) Top-Bead width, (b) Top-Bead height, (c) Upper hardness, (d) Bottom hardness, (e) HAZ hardness, and (f) Dilution Ratio.

### 5.2. Optimization for Welding Process of 9% Ni Steel

The MOO (multi-objective optimization) algorithm to be applied in this study is a technique used to search for non-dominant solutions. This process is derived in previous research [7,28–30]. The program schematic diagram of the MOO optimization method is shown in Figure 10, and MATLAB, which is a commercial numerical analysis program, was used to apply and modify the optimization method. To optimize the welding process variables where the hardening of a weldment has occurred, the same 180 data points in Table 9, which were learned in discriminant analysis, were used, and the variables and levels to drive the MOO optimization technique are shown in Table 12.





**Figure 10.** Flow chart for the multi-objective optimization (MOO) method to predict welding parameters.

**Table 12.** MOO algorithm parameters and their values.

Optimal Method		MOO (Multi-Objective Optimization)
Range of Local Parameters	W (Top-Bead Width)	$[-5 \leq \text{Input} \leq +5]$ A
	H (Top-Bead Height)	$[-1 \leq \text{Input} \leq +1]$ V
Range of Constraints	S (Welding Speed)	$[-0.05 \leq \text{Input} \leq +0.05]$ m/min
	$D_i$ (Dilution Ratio)	$D_i \leq 15.0\%$
Fitness Factor	Population Size	50, 60, 70, 80, 90, 100
Solver		Constrained nonlinear minimization
Algorithm		Trust region reflective algorithm
Derivatives		Gradient supplied

In the MOO technique, the range of flux cored arc welding process parameters was selected from the minimum [150 A, 21 V, 0.3 m/min] to the maximum [170 A, 25 V, 0.4 m/min]. Those conditions are as same as previous research [7], which used “solidification crack susceptibility” as the criteria of welding performance.

The objective function is a mathematical model of the characteristics of a system, and the constraint indicates the conditions that system variables can have. Therefore, Equations (12)–(14) represent the objective function  $f(x)$  of an arbitrary system having  $x$  as a variable, and the constraints and ranges required to optimize this function [31].

$$\text{Optimize } f(C, V, S) \quad (12)$$

$$g(C, V, S) \quad (13)$$

$$D_i < 15.0 \quad (14)$$

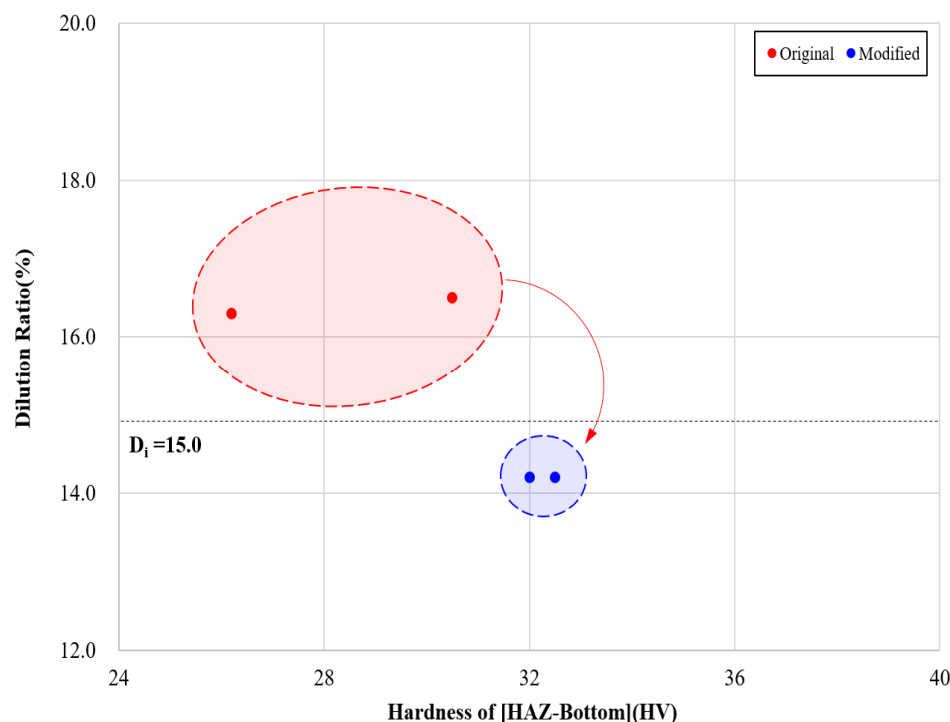
Based on the optimization procedure built as described above, Tests No. 2 and 6 were selected to follow the MOO algorithm and Table 13 shows the welding process variables, expected welding factors, and discrimination results that have been modified to satisfy the constraints according to the optimization procedure.

Figure 11 tried to confirm the possibility of hardening of a weldment by applying the modified input variables, and the effectiveness of optimizing the welding process for 9% Ni steel was confirmed by performing a comparative analysis with the hardening of a weldment caused by the existing input variables. As a result, it was confirmed that the two raw data points selected in the flux cored arc welding process satisfy the dilution ratio of

15.0% or less, which is the limiting condition for hardening of a weldment, and the quality degradation characteristics appearing in the previous process variables were resolved by the modified process variables.

**Table 13.** Results of welding parameters modified by optimization process.

Test No.	Original			Modified			Welding Factors						Group
	C	V	S	C	V	S	W	H	H <sub>U</sub>	H <sub>B</sub>	H <sub>H</sub>	D <sub>i</sub>	
2	150.0	23.0	0.3	151.1	20.2	0.35	8.6	2.6	257.5	286.1	334.0	14.2	Regardless
6	160.0	25.0	0.3	164.9	24.0	0.25	11.8	3.1	259.9	290.5	344.7	14.2	Regardless



**Figure 11.** Weldment hardening distributions using modified input parameters.

## 6. Conclusions

This study attempted to optimize the welding process for 9% Ni steel, which is dominantly used in the LNG storage tank industry. After establishing the criteria for hardening of a weldment in the process, conducting learning in the discriminant function, and optimizing the process variables for hardening of a weldment using the discriminant group, the following conclusions were obtained:

- (1) Appropriate weldability of a weldment was confirmed by measuring the bead geometry, mechanical strength, welding area of a weldment derived from the flux cored arc welding test. It was found the hardening of a weldment depends on the concentration of arc electromagnetic force applied to the weldment and the ratio of an area mixed with a wire after melting. In addition, when a weldment hardening index of 15.0% or more is calculated, the group that needs to consider quality deterioration for weldment hardening is classified, so quality deterioration characteristics according to dilution ratio have been established.
- (2) To determine the weldment hardening phenomenon of 9% Ni steel caused by welding process variables, the quality deterioration characteristics were learned through the SVM technique, and it was determined whether the group with quality deterioration could be accurately identified. As a result, it was confirmed that a group with the hardening of a weldment was predicted 100% repeatedly. This result was reflected, and it was used as a procedure to determine the deterioration of weldment quality.

- (3) A response surface method mathematical prediction model was developed to apply an objective function to optimize the welding process variables where quality deterioration occurs, and it was used in a multi-purpose optimization algorithm. The mathematical model for predicting each factor shows predictive performance in the range of 72.4% to 98.9%. The lowest performance of 72.4% was confirmed in the model predicting the hardness of the lower part of the weld, and the highest performance of 98.9% was confirmed in the model predicting the bead width. By entering the raw data of weldment hardening into the optimization algorithm created by the objective function and constraint conditions, the quality degradation characteristics contained in the process variables were supplemented.
- (4) Test No. 2 and 6 of Raw Data in which weld hardening occurred were selected and adjusted according to the MOO algorithm, and corrected to satisfy the dilution rate limiting condition by the optimization procedure. As a result of inputting the input variables complemented with the deterioration characteristics into the mathematical model of the reaction surface, calculating the predicted welding factor, and re-entering the output variables into the discrimination system, hardening of the welded part is expected. It was confirmed that the dilution rate of all the raw data was less than 15% and that the deterioration of quality was offset.

**Author Contributions:** Conceptualization, M.P. and K.C.; methodology, M.P.; software, C.P. and K.C.; validation, K.C., J.K. (Jisun Kim); formal analysis, M.P.; investigation, M.P.; resources, J.K. (Jaewoong Kim); data curation, M.P.; writing—original draft preparation, M.P.; writing—review and editing, M.P., J.K. (Jisun Kim), C.P., J.K. (Jaewoong Kim), and K.C.; visualization, C.P.; supervision, J.K. (Jaewoong Kim), K.C.; project administration, J.K. (Jaewoong Kim), K.C.; funding acquisition, J.K. (Jaewoong Kim). All authors have read and agreed to the published version of the manuscript.

**Funding:** This study has been conducted with the support of the Korea Institute of Industrial Technology as “The dynamic parameter control based smart welding system module development for the complete joint penetration weld (kitech EH-21-0003).”

**Institutional Review Board Statement:** Not applicable.

**Informed Consent Statement:** Not applicable.

**Data Availability Statement:** The data presented in this study are available on request from the corresponding author.

**Conflicts of Interest:** The authors declare no conflict of interest.

## References

- IMO. *Regulations to Reduce Air Pollution from Ships and the Review of Fuel Oil Availability*; IMO: London, UK, 2016.
- Kim, K.; Park, K.; Roh, G.; Ghun, K. Case Study on Boil-Off Gas (BOG) Minimization for LNG Bunkering Vessel Using Energy Storage System (ESS). *J. Mar. Sci. Eng.* **2019**, *7*, 130. [[CrossRef](#)]
- Lee, Y.H. Analysis of the Characteristics of Reformer for the Application of Hydrogen Fuel Cell Systems to LNG Fueled Ships. *J. Korean Soc. Mar. Environ. Saf.* **2021**, *27*, 135–144. [[CrossRef](#)]
- Peng, Y.; Zhao, X.; Zuo, T.; Wang, W.; Song, X. A systematic literature review on port LNG bunkering station. *Transp. Res. Part D Transp. Environ.* **2021**, *91*, 102704. [[CrossRef](#)]
- Chang, W.S.; Kim, K.C.; Kim, Y.C.; Kim, S.R.; Kim, W.S. Ni alloy welding consumables for 9% Nickel steel. *Korean Weld. Join Soc.* **1998**, *16*, 25–37.
- ASTM E23. *Standard Test Methods for Notched Bar Impact Testing of Metallic Materials*; ASTM International: West Conshohocken, PA, USA, 2007; pp. 1–6.
- Park, M.; Kim, J.; Pyo, C.; Son, J.; Kim, J. Research for the Optimal Flux-Cored Arc Welding Process of 9% Nickel Steel Using Multi Object Optimization with Solidification Crack Susceptibility. *Materials* **2021**, *14*, 1659. [[CrossRef](#)] [[PubMed](#)]
- Yun, T.; Oh, W.; Lee, B.; Lee, C.; Na, H.; Choi, J.; Kim, I. A Study on Optimization of Fillet in Laser Welding Process for 9% Ni Steel Using Gradient-Based Optimization Algorithm. *J. Weld. Join.* **2020**, *38*, 485–492. [[CrossRef](#)]
- Na, K.; Lee, C.; Park, J.; Cho, M. A Comparison of Hot Cracking in GTAW and FCAW by Applying Alloy 625 Filler Materials of 9% Ni Steel. *J. Weld. Join.* **2019**, *37*, 357–362. [[CrossRef](#)]
- Kim, B.; Park, J.; Lee, J.; Kim, M. Study on the Initial Design of an LNG Fuel Tank using 9 wt. % Nickel Steel for Ships and Performance Evaluation of the Welded Joint. *J. Weld. Join.* **2019**, *37*, 555–563. [[CrossRef](#)]

11. Watanabe, I.; Suzuki, M.; Matsuda, Y.; Tagawa, H.; Matsui, K.; Shimada, S. Fracture toughness of 9% Ni steel and safety of LNG storage tank against brittle fracture. *Nippon Kokan Tech. Rep.* **1984**, *42*, 2–10.
12. Liu, X.; Athanasiou, C.E.; Padture, N.P.; Sheldon, B.W.; Gao, H. A machine learning approach to fracture mechanics problems. *J. Acta Mater.* **2020**, *190*, 105–112. [[CrossRef](#)]
13. Oliveira, J.P.; Curado, T.M.; Zeng, Z.; Lopes, J.G.; Rossinyol, E.; Park, J.M.; Schell, N.; Braz Fernandes, F.M.; Kim, H.S. Gas tungsten arc welding of as-rolled CrMnFeCoNi high entropy alloy. *Mater. Des.* **2020**, *189*, 1–12. [[CrossRef](#)]
14. Oliveira, J.P.; Crispim, B.; Zeng, Z.; Omori, T.; Braz Fernandes, F.M.; Mianda, R.M. Microstructure and mechanical properties of gas tungsten arc welded Cu-Al-Mn shape memory alloy rods. *J. Mater. Process. Technol.* **2019**, *271*, 93–100. [[CrossRef](#)]
15. Kim, M.; Shin, S.; Kim, D.; Lee, S. A Study on the Algorithm for Determining Back Bead Generation in GMA Welding Using Deep Learning. *J. Weld. Join.* **2018**, *36*, 74–81. [[CrossRef](#)]
16. Zhu, H.; Ge, W.; Liu, Z. Deep Learning-Based Classification of Weld Surface Defects. *Appl. Sci.* **2019**, *9*, 3312. [[CrossRef](#)]
17. Oh, D.J.; Lee, J.M.; Noh, B.J.; Kim, W.S.; Ando, R.; Matsumoto, T.; Kim, M.H. Investigation of fatigue performance of low temperature alloys for liquefied natural gas storage tanks. *J. Mech. Eng.* **2015**, *229*, 1–15. [[CrossRef](#)]
18. Kourshid, A.F.M.; Ghanem, M. Using the welding parameters to improve the mechanical properties of Liquefied Natural Gas storage tank welded joint. *IOSR J. Mech. Civil Eng. IOSR-JMCE* **2012**, *4*, 32–39. [[CrossRef](#)]
19. *Technical Report 9% Nickel Steel: For Use at Cryogenic Temperatures*; ArcelorMittal: Chicago, IL, USA, 2010.
20. Kobelco Welding of America Inc. Kobelco's Welding Consumables for LNG Storage Tanks Made of 9% Ni Steel. *Kobelco Weld.* **2011**, *14*, 3–8.
21. Byun, J.O.; Choi, Y.H. Stair locomotion method of quadruped robot using genetic algorithm. *J. Korea Inst. Electron. Commun. Sci.* **2015**, *10*, 1039–1047. [[CrossRef](#)]
22. Kim, W.W. *A Multi-Objective Genetic Algorithm Using Sequential Surrogate Models*; Hanyang University Graduate School: Seoul, Korea, 2012.
23. KoreaScience. *Welding and Bonding Hand Book—Process and Thermal Processing*; KoreaScience: Seoul, Korea, 2007.
24. Kim, Z.H. A Comparative Study of Classification Techniques Using Forest Cover Type Data: Discriminant Analysis, Logistic Regression, Neural Network, Decision Tree. Master's Thesis, Chung-Ang University, Seoul, Korea, 2012, unpublished.
25. Amrine, D.E.; White, B.J.; Larson, R.L. Comparison of classification algorithms to predict outcomes of feedlot cattle identified and treated for bovine respiratory disease. *Comput. Electron. Agric.* **2014**, *105*, 9–19. [[CrossRef](#)]
26. Knowles, J.D.; Corne, D.W. Approximating the nondominated front using the pareto archived evolution strategy. *Evol. Comput.* **2000**, *8*, 149–172. [[CrossRef](#)]
27. Vapnik, V.N. *The Nature of Statistical Learning Theory*; Springer: Berlin/Heidelberg, Germany, 1999.
28. Deb, K.; Agrawal, S.; Pratap, A.; Meyarivan, T. A fast elitist non-dominated sorting genetic algorithm for multi-objective optimization: NSGA-II. *Lect. Notes Comput. Sci.* **2000**, *1917*, 849–858.
29. Zitzler, E.; Deb, K.; Thiele, L. Comparison of multiobjective evolutionary algorithms: Empirical results. *Evol. Comput.* **2000**, *8*, 173–195. [[CrossRef](#)] [[PubMed](#)]
30. Veldhuizen, D.A.V.; Lamont, G.B. On measuring multiobjective evolutionary algorithm performance. *Evol. Comput.* **2000**, *1*, 204–211.
31. Deb, K.; Pratap, A.; Agarwal, S.; Meyarivan, T.A. A fast and elitist multi objective genetic algorithm: NSGA-II. *IEEE Trans. Evol. Comput.* **2002**, *6*, 182–197. [[CrossRef](#)]